Large Lithium Isotopic Variations in Minerals from Peridotite Xenoliths from the Eastern North China Craton

Yan Xiao,[1,*] *Hong-Fu Zhang,*[1,2] *Etienne Deloule,*[3] *Ben-Xun Su,*[1] *Yan-Jie Tang,*[1] *Patrick Asamoah Sakyi,*[4] *Yan Hu,*[1] *and Ji-Feng Ying*[1]

1. State Key Laboratory of Lithospheric Evolution, Institute of Geology and Geophysics, Chinese Academy of Sciences, PO Box 9825, Beijing 10029, China; 2. State Key Laboratory of Continental Dynamics, Department of Geology, Northwest University, Xi'an 710069, China; 3. Centre National de la Recherche Scientifique, Centre de Recherches Petrographiques et Geochimiques, BP20, 54501 Vandoeuvre-Les-Nancy Cedex, France; 4. Department of Earth Science, University of Ghana, PO Box LG 58, Legon-Accra, Ghana

ABSTRACT

To investigate the effects of melt-rock interaction on Li isotope fractionation, we report in situ Li concentrations and δ^7Li of olivine (Ol), orthopyroxene (Opx), and clinopyroxene (Cpx) for six peridotite xenoliths from the eastern North China Craton. These xenoliths contain two lherzolites, two Cpx-rich lherzolites, and two wehrlites and are variably metasomatized. Lithium isotope zonation is observed in most peridotite minerals. The majority of Cpx grains display isotopically light cores with lower Li concentrations than the heavy rims. However, the Opx grains show a different style of zonation from Cpx, where higher Li concentrations in the cores are associated with much lighter δ^7Li. Olivines in most peridotites have a restricted range of Li concentration and δ^7Li within individual grains, whereas the olivines in a lherzolite show isotopically light cores (−10.3) with high Li concentrations (2.3 ppm) and heavy rims (5.5) with low Li concentrations (1.7 ppm). These Li isotopic variations in mineral phases may reflect the combined effects of diffusion-driven kinetic fractionation of Li isotopes during melt/fluid-peridotite interactions and slow cooling. Intersample heterogeneity of Li isotopes is also apparent. Olivine with forsterite (Fo) content of 91.3 in one lherzolite sample has "normal" mantle-like Li concentrations (1.1~2.4 ppm) and light δ^7Li (−10.3~5.5), while Ol with Fo content of 89.7 in another lherzolite has slightly high Li concentrations (2.0~3.0 ppm) but similar δ^7Li (1.6~6.4) relative to normal mantle. Olivines in Cpx-rich lherzolites have lower Fo contents (83.8–87.5), higher Li concentrations (1.4~4.5 ppm), and heavier δ^7Li (5.0~22.0) than those in lherzolites and normal mantle. The δ^7Li_{Ol} value correlates positively with Li concentration and negatively with Fo from lherzolites to Cpx-rich lherzolites, indicating a reaction between lherzolites and melts with isotopically heavy Li- and Fe-rich signatures. By contrast, olivines in wehrlites have extremely lower Fo contents (82.2~83.2) and higher Li concentrations (2.4~4.2 ppm) than those in normal mantle, while their δ^7Li values are within the range of normal mantle, reflecting metasomatism of the peridotites by asthenospheric melt. Overall, the large intragrain and intersample variations in Li concentrations and isotopic compositions reflect kinetic isotope fractionation during multiple metasomatisms.

Introduction

The two stable isotopes of Li, ^{6}Li and ^{7}Li, have the biggest relative mass difference (~17%) of any isotope pair aside from hydrogen and deuterium. This leads to large variability in the isotopic compositions of Li at low temperature, with δ^7Li ranging from 56 in some sedimentary pore fluids (You et al. 2003) to −22 in orogenic eclogites (Marschall et al. 2007). The large relative mass difference in the Li isotope system also leads to significant isotopic fractionations (40‰) at high temperature, on the basis of studies of contact aureoles, peridotites, and phenocrysts in lavas (Lundstrom et al. 2005; Beck et al. 2006; Teng et al. 2006; Jeffcoate et al. 2007; Marks et al. 2007; Rudnick and Ionov 2007; Parkinson et al. 2007; Tang et al. 2007; Wagner and

Manuscript received January 7, 2014; accepted December 8, 2014; electronically published January 20, 2015.

* Author for correspondence; e-mail: xiaoyan@mail.iggcas.ac.cn.

[The Journal of Geology, 2015, volume 123, p. 79–94] 0022-1376/2015/12301-0005$15.00. DOI:10.1086/680222

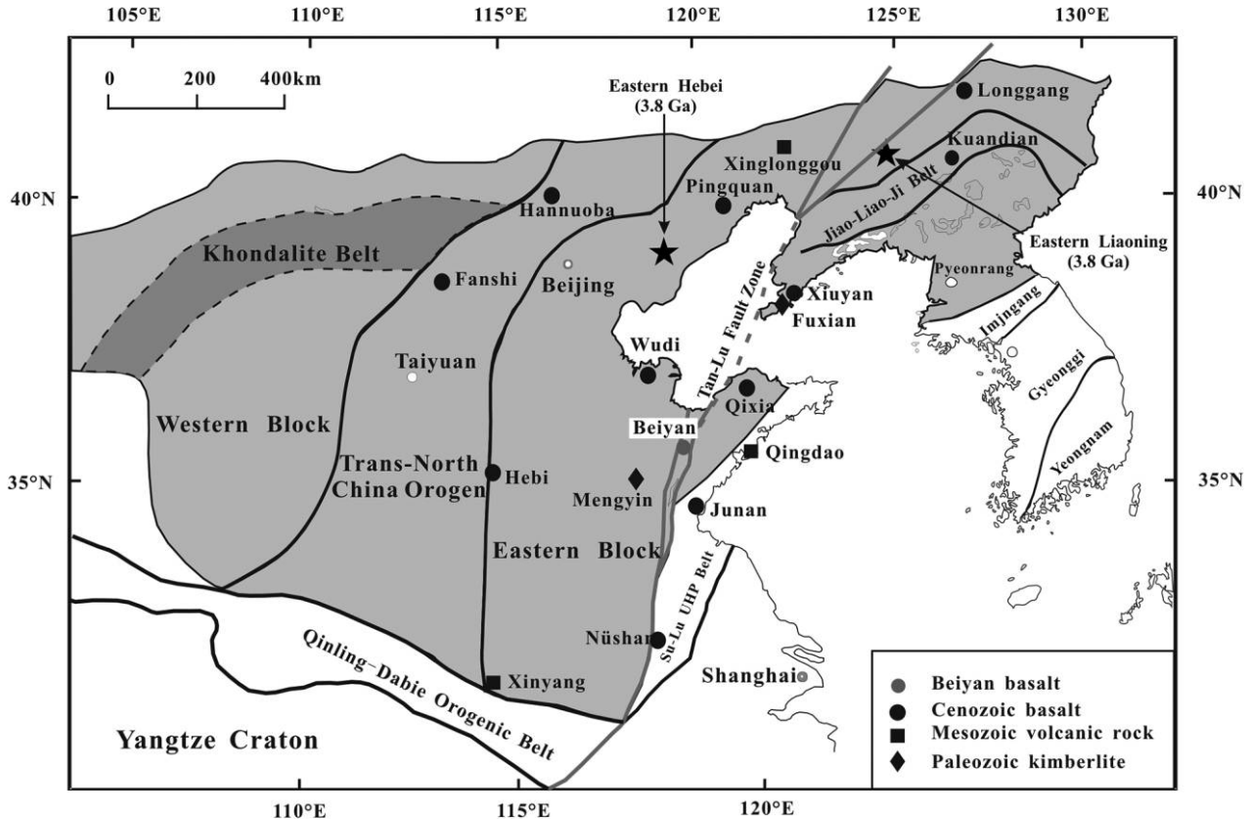

Figure 1. Simplified geological map showing major tectonic units, xenolith localities, and major volcanic rocks in the North China Craton (modified from Zhao et al. 2008). A color version of this figure is available online.

Deloule 2007; Aulbach et al. 2008; Ionov and Seitz 2008), which contrasts with the relatively uniform δ^7Li of mid-ocean ridge basalts (MORBs; 2–6; Tomascak et al. 2008).

Previous studies of peridotite xenoliths have reported a wide range of Li isotope fractionation between olivine (Ol) and clinopyroxene (Cpx), with $\Delta^7Li_{Ol\text{-}Cpx}$ values of up to 3.5‰ (Seitz et al. 2004), −2.4‰ to 1.2‰ (Magna et al. 2006), −3.6‰ to 13.5‰ (Jeffcoate et al. 2007), 3‰ to 23‰ (Rudnick and Ionov 2007), 0.3‰ to 15.8‰ (Wagner and Deloule 2007), 8.6‰ to 12.7‰ (Tang et al. 2007), 1.8‰ to 11.9‰ (Aulbach and Rudnick 2009), 0.5‰ to 23.2‰ (Tang et al. 2011), and 24.2‰ (Ionov and Seitz 2008). These large intermineral fractionations in natural samples are generally attributed to diffusion-driven kinetic effects. However, the nature of Li diffusion processes during the interaction of peridotites with percolating melts and/or host magmas (Jeffcoate et al. 2007; Rudnick and Ionov 2007; Aulbach and Rudnick 2009; Su et al. 2012), during their interaction with slab-derived low δ^7Li melt (Nishio et al. 2004; Tang et al. 2007, 2010, 2012, 2014; Zhang et al. 2010), or during the cooling of magmatic systems (Ionov and Seitz 2008; Gao et al. 2011) is currently disputed. Dohmen et al. (2010) reported a complex diffusion behavior of Li, indicating that two mechanisms of Li diffusion (faster and slower mechanisms) operate simultaneously. They suggested that the faster mechanism of Li diffusion is unlikely to be dominant in most natural systems. Diffusion dominated by the slower mechanism will occur on average at a rate that is about an order of magnitude faster than diffusion of Fe, Mg, and most other divalent cations in Ol and much slower than the rates of diffusion in Cpx and plagioclase crystals under the same conditions (Dohmen et al. 2010). Thus, fractionation of Li isotopes by diffusion is likely to be a transient phenomenon that produces isotopically zoned crystals. Therefore, in situ Li isotopic analysis of mantle minerals may provide more constraints on the potential factors controlling the Li isotope fractionation.

Here, we report in situ Li concentrations and isotopic compositions of Ol, Cpx, and orthopyroxene (Opx) from well-characterized and variably metasomatized peridotite xenoliths from the east-

Table 1. Major Elemental Compositions (wt%) of Minerals in Beiyan Peridotites

Sample, mineral	SiO_2	TiO_2	Al_2O_3	Cr_2O_3	FeO	MnO	MgO	CaO	Na_2O	NiO	Total	Fo
CLB05-31:												
Ol	41.2				8.54	.08	49.6	.05		.28	99.8	91.3
Opx	55.5	.11	3.56	.47	5.39	.10	33.6	.65	.00	.07	99.5	91.8
Cpx	53.3	.18	4.98	.92	2.22	.09	16.0	20.5	.00	.05	98.2	92.9
CLB05-50:												
Ol	41.2				9.85	.09	47.5	.02		.29	99.0	89.7
Opx	55.7	.11	3.98	.22	6.37	.12	33.0	.39	.00	.00	99.9	90.3
Cpx	52.2	.77	6.55	.67	2.28	.06	14.5	20.5	.00	.08	97.6	92.0
CLB05-25:												
Ol	40.1				12.2	.17	47.3	.06		.35	100	87.5
Opx	54.4	.08	4.37	.30	7.33	.20	32.0	.61	.10	.12	99.6	88.7
Cpx	52.9	.39	6.11	.65	3.28	.15	14.9	18.7	2.06	.05	99.1	89.1
CLB05-15:												
Ol1	39.1				15.5	.18	44.2	.06		.35	99.4	83.7
Ol2	39.2				15.3	.20	44.4	.05		.34	99.5	83.9
Ol3	38.0				15.6	.25	44.1	.07		.31	98.3	83.6
Ol4	39.0				15.4	.24	44.7	.05		.31	99.7	83.9
Ol5	38.9				15.2	.25	43.4	.07		.30	98.1	83.7
Ol6	39.1				15.5	.22	44.4	.08		.31	99.6	83.8
Opx	52.5	.19	4.66	.32	9.56	.18	30.2	.80	.08	.08	98.6	85.1
Cpx	38.3	.00	.00	.00	15.7	.18	43.7	.06	.00	.32	98.4	83.3
CLB05-80:												
Ol	40.5				16.0	.15	43.8	.07		.16	101	83.2
Cpx	50.9	1.25	7.96	.37	4.50	.10	14.2	19.5	.00	.01	98.8	85.0
CLB05-35:												
Ol	40.1				16.9	.16	43.3	.09		.15	101	82.2
Cpx	48.5	2.47	8.62	.05	4.70	.07	13.1	20.6	.00	.01	98.1	83.3

Note. Cpx = clinopyroxene; Fo = $100 \cdot Mg^{2+}/(Mg^{2+} + Fe^{2+})$; Ol = olivine; Opx = orthopyroxene; Spl = spinel.

ern North China Craton. We use these data together with previously published data to investigate the origin of the intragrain and intersample Li isotope fractionation and the effects of mantle metasomatism on Li isotopic compositions of peridotites.

Geological Background and Samples

The North China Craton is bounded by the Central Asia Orogenic Belt to the north and the Qinling-Dabie-Sulu high/ultrahigh-pressure metamorphic belt to the south and east (fig. 1; Zhao et al. 2008). The craton is divided into three regions: the Western Block, the Eastern Block, and the Trans–North China Orogen. The Trans–North China Orogen was formed by the collision between the Eastern Block and the Western Block at ~1.85 Ga, marking the final amalgamation of the North China Craton (Zhao et al. 2008). The Tan-Lu fault zone, a major wrench fault in northeastern Asia, cuts through the eastern part of the North China Craton and extends deep into the subcontinental lithospheric mantle (Peng et al. 1986; Xu et al. 1987, 1993, 1996; Zheng et al. 1998, 2007).

Within and adjacent to the Tan-Lu fault zone, large amounts of Cenozoic alkali basalts occur, such as at the Changle-Linqu volcanic field and the Yishui and Qixia volcanic fields (fig. 1). Beiyan basalts, one of the basalts in the Changle-Linqu volcanic field, contain abundant mantle peridotite xenoliths, including lherzolite, Cpx-rich lherzolite, and wehrlite (Xiao et al. 2010). The lherzolites, with forsterite (Fo) contents (~90) of Ol and spoon-shaped to slightly light rare earth element–enriched patterns, reflect a low degree of melt extraction

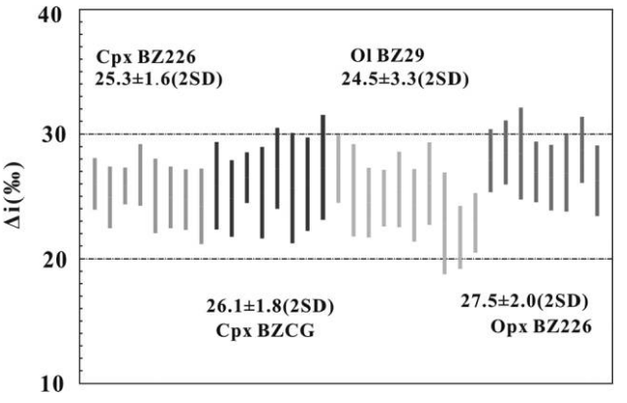

Figure 2. Standard Li isotopic variation throughout the analyses with 2σ error bars. Cpx = clinopyroxene; Ol = olivine; Opx = orthopyroxene.

Table 2. In Situ Analytical Data by Secondary Ion Mass Spectroscopy for the Beiyan Peridotites

Sample	Mineral	Position	Li (ppm)	δ^7Li (‰)	2σ	Fo	Corrected δ^7Li (‰)[a]	Size of grain (μm)[b]
CLB05-31	Ol1	Rim	1.78	4.0	1.4	90.7		356
			2.32	−3.9	1.9			
			2.28	−8.4	1.7			
		Core	2.34	−9.5	1.6			
	Ol2	Rim	1.16	4.8	1.9			857
			1.66	5.5	1.6			
			2.14	−3.4	1.2			
		Core	2.33	−10.2	1.5			
			2.31	−10.3	1.4			
			2.10	−3.9	1.8			
			1.61	4.1	1.3			
		Rim	1.14	3.1	2.5			
	Ol3	Rim	2.22	−1.9	.9			788
		Core	2.38	−9.9	1.3			
	Cpx1	Rim	2.22	−18.2	1.7			143
			1.99	−20.3	2.6			
			2.32	−22.7	2.3			
		Core	2.38	−26.3	1.8			
	Cpx2	Rim	3.54	−9.8	1.9			26
		Core	3.97	−11.5	1.9			
	Cpx3	Rim	3.75	−11.4	1.0			143
			4.12	−11.1	1.0			
			3.61	−14.3	1.2			
		Core	3.25	−18.6	1.2			
	Opx1	Rim	1.83	−5.4	1.7			161
			2.74	−7.5	1.8			
			4.55	−7.7	1.2			
		Core	6.35	−8.8	.7			
	Opx2	Rim	.70	−7.1	4.2			277
			1.22	−5.4	3.2			
		Core	2.88	−7.2	2.2			
CLB05-50	Ol1	Rim	2.21	5.5	1.3	89.6		144
			2.42	6.4	1.3			
		Core	2.37	5.2	.8			
	Ol2	Rim	3.02	6.0	1.5			614
			1.95	6.3	2.0			
			2.41	4.0	.9			
			2.42	2.1	1.5			
		Core	2.14	1.6	1.2			
	Cpx1	Rim	2.79	1.5	1.6			458
			2.31	.3	1.0			
			2.27	4.3	.6			
		Core	2.29	1.5	1.4			
	Cpx2	Rim	3.13	4.4	1.1			91
			3.46	5.5	.8			
		Core	3.50	1.3	1.4			
	Opx1	Rim	.55	9.7	2.9			1582
			1.12	7.0	1.7			
			5.68	−3.0	.8			
		Core	3.25	−10.6	1.1			
			2.31	−4.4	1.5			
		Core	3.30	−12.2	1.5			
			3.83	−6.3	1.4			
			3.47	1.7	1.2			
		Rim	2.08	6.8	1.7			
	Opx2	Core	2.91	12.3	1.4			
	Opx3	Core	.91	8.6	2.7			
CLB05-25	Ol1	Rim	2.47	14.5	1.4	87.5	11.2	470
			2.54	12.9	1.3	87.5	9.6	
			3.00	8.3	1.5	87.5	5.0	
		Core	3.00	9.3	1.1	87.5	6.0	
	Ol2	Rim	2.51	15.6	1.1	87.5	12.3	118
			2.32	16.0	1.3	87.5	12.7	
		Core	2.46	16.6	1.2	87.5	13.3	

Table 2 (*Continued*)

Sample	Mineral	Position	Li (ppm)	δ^7Li (‰)	2σ	Fo	Corrected δ^7Li (‰)[a]	Size of grain (μm)[b]
	Cpx1	Rim	3.84	7.5	.9			163
			3.17	5.0	1.2			
			3.21	1.5	1.0			
		Core	2.62	−1.3	.9			
	Cpx2	Rim	3.24	6.2	1.2			215
			3.27	.3	.9			
		Core	2.79	−2.0	1.3			
	Opx1	Rim	1.25	3.8	2.2			319
			1.65	5.9	1.8			
			3.80	4.3	1.4			
		Core	5.48	−6.8	1.2			
	Opx2	Rim	2.81	7.6	1.8			273
			3.24	8.4	1.5			
			4.65	1.9	1.3			
		Core	5.06	−.7	1.2			
CLB05-15	Ol1	Rim	1.44	29.6	1.6	83.7	21.4	151
			1.61	30.2	1.8	83.7	22.0	
		Core	2.35	29.5	2.2	83.7	21.2	
	Ol2	Rim	4.41	17.5	.9	83.9	9.7	433
			4.49	15.3	1.2	83.9	7.4	
		Core	2.61	21.5	1.0	83.9	13.7	
	Ol3	Core	2.63	28.9	1.8	83.6	20.6	
	Ol4	Core	2.58	23.6	1.6	83.9	15.7	
	Ol5	Core	3.02	15.7	1.7	83.7	7.6	
	Ol6	Core	2.63	20.9	.9	83.8	12.8	
	Cpx1	Rim	7.08	2.1	1.1			176
			8.33	2.7	1.0			
		Core	6.91	−3.0	.9			
	Cpx2	Rim	7.56	1.6	.4			175
			8.68	−.5	.7			
		Core	7.96	−1.2	1.1			
	Opx1	Rim	1.17	2.9	2.0			496
			2.25	1.9	1.8			
		Core	5.60	−2.8	1.1			
	Opx2	Rim	.60	.8	2.9			
		Core	.59	3.3	2.8			
CLB05-80	Ol1	Rim	3.00	8.9	1.0	83.2	.0	852
			2.42	12.0	2.1	83.2	3.2	
			3.21	12.2	1.3	83.2	3.3	
			3.18	13.3	1.5	83.2	4.5	
		Core	3.21	12.4	1.5	83.2	3.6	
		Core	3.65	14.1	1.0	83.2	5.2	
			3.20	13.6	1.1	83.2	4.8	
			2.98	13.5	1.6	83.2	4.7	
			3.34	17.4	1.2	83.2	8.6	
			3.25	8.0	1.4	83.2	−.8	
		Rim	3.17	8.6	1.7	83.2	−.2	
	Ol2	Rim	3.55	2.9	1.2	83.2	−5.9	84
		Core	2.77	12.4	1.3	83.2	3.5	
	Ol3	Rim	4.16	6.3	1.3	83.2	−2.5	189
		Core	3.32	12.4	1.7	83.2	3.6	
	Ol4	Rim	3.00	9.0	1.5	83.2	.1	492
			2.89	10.6	1.4	83.2	1.8	
			3.20	13.3	1.2	83.2	4.5	
			2.78	12.3	1.6	83.2	3.4	
			2.76	13.4	1.1	83.2	4.6	
			2.83	13.0	1.0	83.2	4.2	
		Core	2.72	13.3	1.6	83.2	4.5	
	Cpx1	Rim (S-CPX)	1.16	1.1	2.3			489
			1.20	−2.4	4.2			
			3.58	−9.2	1.0			
			5.50	.7	.8			
		Core (C-CPX)	6.00	4.2	1.2			

Table 2 (*Continued*)

Sample	Mineral	Position	Li (ppm)	δ^7Li (‰)	2σ	Fo	Corrected δ^7Li (‰)[a]	Size of grain (μm)[b]
	Cpx2	Rim (C-CPX)	1.50	2.3	2.3			525
			3.95	3.9	3.5			
			.76	1.4	2.3			
			1.48	−1.0	3.7			
			4.46	−13.2	1.1			
		Core (C-CPX)	4.92	−14.4	1.2			
	Cpx3	Rim (S-CPX)	1.45	1.9	2.6			557
			1.82	7.0	4.4			
			.99	2.1	2.3			
		Core (S-CPX)	.73	.5	6.3			
CLB05-35	Ol1	Rim	3.56	15.8	1.0	82.2	5.6	196
			3.53	15.3	1.2	82.2	5.2	
			3.36	15.0	1.2	82.2	4.9	
		Core	3.03	16.5	1.7	82.2	6.4	
	Ol2	Core	3.30	14.1	1.4	82.2	4.0	
	Cpx1	Rim	7.17	.0	.9			465
			6.70	−1.2	.6			
			6.87	−6.5	1.0			
		Core	4.60	−11.3	.8			
	Cpx2	Rim	6.35	−3.7	.8			125
			6.07	−4.2	.8			
			5.17	−3.4	1.1			
		Core	6.29	−1.9	1.1			

Note. C-CPX = clear Cpx; Cpx = clinopyroxene; Fo = $100 \cdot Mg^{2+}/(Mg^{2+} + Fe^{2+})$; Ol = olivine; S-CPX = sieve-textured Cpx; Opx = orthopyroxene.

[a] The matrix effect for Ol from Cpx-rich lherzolites and wehrlites is deducted according to the calculation by Bell et al. (2009).

[b] Represents the distance from the rim spot to the core spot for each analyzed grain.

overprinted by recent metasomatism. They represent fragments of newly accreted lithospheric mantle that make up much of the Late Mesozoic–Cenozoic lithosphere beneath the eastern North China Craton (Zheng et al. 1998, 2007; Ying et al. 2006; Chu et al. 2009; Xiao et al. 2010; Zhang et al. 2011). The Cpx-rich lherzolite and wehrlite were produced by the interaction of lherzolites with melts, as indicated by partially or completely replaced Opx with Cpx and low Fo contents (<88; Xiao et al. 2010).

In this study, Li concentrations and isotopic compositions were determined in situ for mineral separates (Ol, Cpx, and Opx) in two lherzolites, two Cpx-rich lherzolites, and two wehrlites. All samples show little effects of surface alteration and were selected from a larger collection on the basis of their large diameters (~15 cm). Lherzolite CLB05-31, with Fo content of 91.3, shows a granuloblastic microstructure, while lherzolite CLB05-50, with Fo content of 89.7, is porphyroclastic, with big Opx (2~3 mm) showing exsolution lamellae of Cpx (table 1). The two Cpx-rich lherzolites (CLB05-25 and CLB05-15), with low-Fo (87.5 and 83.8, respectively) olivines, display partial replacement texture of Opx by Cpx (table 1). The two wehrlites (CLB05-80 and CLB05-35), on the other hand, consist of rounded Ol with extremely low Fo contents in Ol (83.2 and 82.2, respectively; table 1) and interstitial sieve-textured Cpx.

Analytical Methods

Major element compositions were obtained by wavelength-dispersive spectrometry using a JEOL JXA8100 electron probe microanalyzer at the Institute of Geology and Geophysics (IGG), Chinese Academy of Sciences, operating at an accelerating voltage of 15 kV with 10-nA beam current, 5-μm beam spot, and 10~30-s counting time on peak (table 1). The precisions of all analyzed elements were better than 1.5%.

Li concentrations and isotope microanalyses were obtained using the Cameca IMS-1280 ion microprobe at the IGG, Chinese Academy of Sciences, following the methods reported in Zhang et al. (2010) and Su et al. (2012). Samples were sputtered with a 13-kV O^- primary beam with a current intensity of 10–20 nA and diameter of 20 μm. Since positive secondary ions accelerated through 10 kV were measured at medium mass resolution ($M/\Delta M$~1100) with a 125-μm aperture, no energy offset was applied, and the energy slit was kept wide open. Before each measurement, the primary beam position,

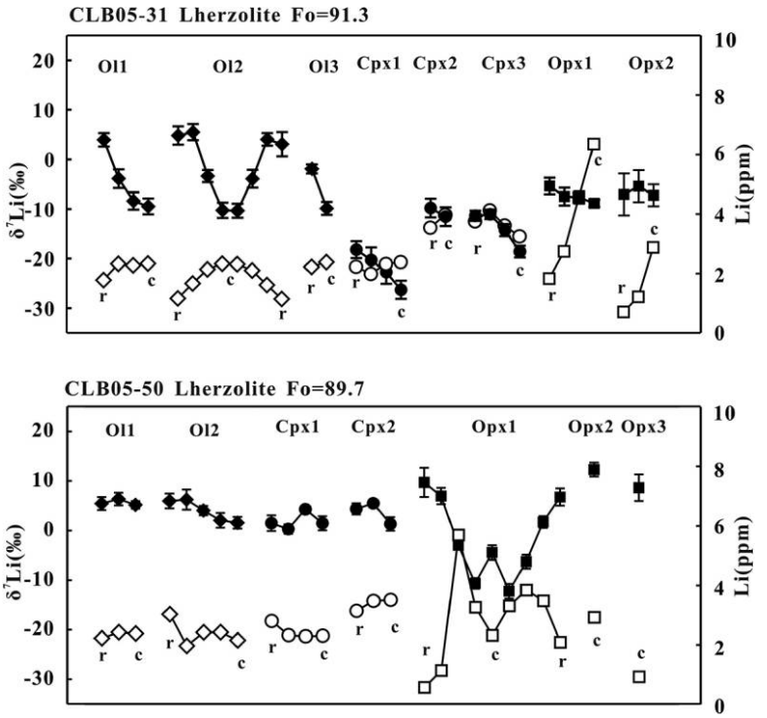

Figure 3. Profiles of Li concentrations and isotopic compositions of olivine (Ol), orthopyroxene (Opx), and clinopyroxene (Cpx) in the Beiyan lherzolites analyzed by secondary ion mass spectroscopy. Open and filled symbols represent Li concentrations and δ^7Li, respectively. c = core; r = rim.

entrance slits, contrast aperture, magnetic field, and energy offset were automatically centered. Secondary ions were counted in monocollection pulse-counting mode. Counting times were 12 s for ^{6}Li, 4 s for background at the 6.5 mass, and 4 s for ^{7}Li in each cycle, with 30–50 cycles per analysis. The counting rate for ^{7}Li ranged from 30,000 to 100,000 cps, depending on the sample Li concentration and primary beam intensity. A 60-s presputtering without raster was applied before analysis. Li isotopic compositions are expressed as δ^7Li relative to the National Institute of Standards L-SVEC standard ($\delta^7\text{Li} = [(^7\text{Li}/^6\text{Li})_{\text{sample}}/(^7\text{Li}/^6\text{Li})_{\text{L-SVEC}} - 1] \times 1000$, with $^7\text{Li}/^6\text{Li}_{\text{L-SVEC}} = 12.0192$). Cpx BZ226 and BZCG, Ol BZ29, and Opx BZ226 (Decitre et al. 2002) were used as standards (fig. 2). For these standards, the measured $\delta^7\text{Li} = -4.7 \pm 0.8$, 10.9 ± 0.9, 4.4 ± 1.0, and -4.2 ± 1.2, respectively, consistent with the recommended values ($\delta^7\text{Li} = -4.1$, 10.5, 4.4 and -4.2, respectively) with analytical error. The external 2σ of the standards and most samples were lower than 2‰ (table 2).

Bell et al. (2009) reported that there was a substantial effect of composition on the ^{7}Li/^{6}Li ratio of Ol measured by secondary ion mass spectroscopy (SIMS). For magnesian Ol ($74 < \text{Fo} < 94$), the effect is a linear function of composition, with δ^7Li increasing by 1.3 for each mole percent decrease in Fo component. Olivines from the Beiyan peridotites show a wide range of Fo contents from 91.3 to 82.2. Ignoring the matrix effects, olivines in the lherzolites have Fo contents similar to those of the standards, whereas olivines in the Cpx-rich lherzolites and wehrlites have low Fo contents, and the δ^7Li values were corrected on the basis of the linear function calculated by Bell et al. (2009). The corrected data are reported in table 2. However, at a mineral scale in each sample, the analyzed Ol is generally homogeneous in major element compositions. As for pyroxene, the effect of matrix composition on δ^7Li in pyroxenes likely may also be a complicating factor, but in this study we are dominantly concerned with intragrain fractionations of pyroxenes. Therefore, the inaccuracies of this approach do not influence our main conclusions.

Results

Representative electron microprobe analyses of Ol, Opx, and Cpx in the Beiyan xenoliths are reported in table 1. In situ Li concentrations and isotopic compositions are reported in table 2.

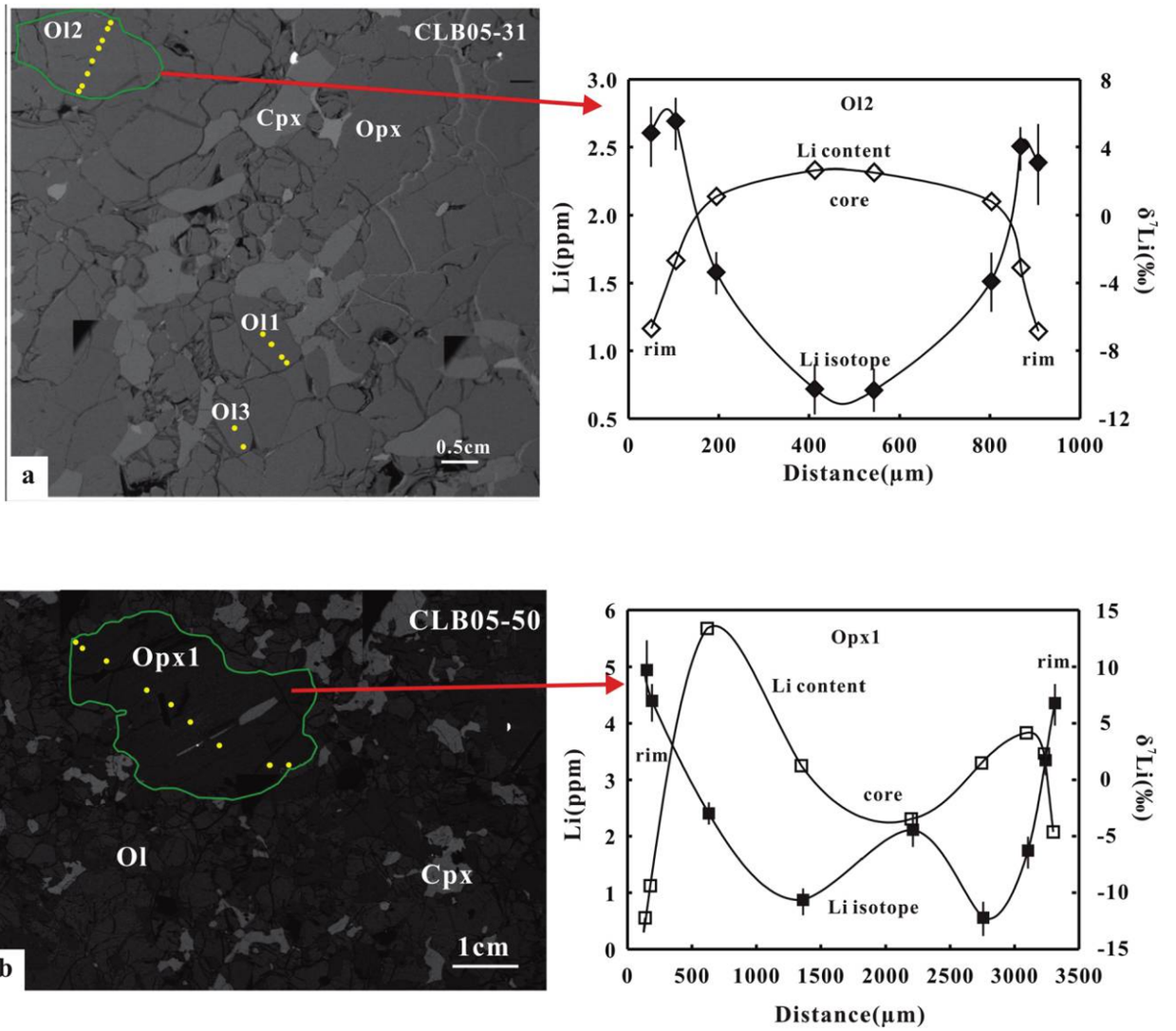

Figure 4. Backscattered electron micrographs of lherzolite CLB05-31 and CLB05-50 showing the position of the Li isotopic and Li concentration measurements by secondary ion mass spectroscopy and corresponding plots of Li isotope (filled diamonds/squares) and concentration (open diamonds/squares) represented as a profile across the olivine (Ol; *a*) and orthopyroxene (Opx; *b*) crystal.

Lherzolite. *Sample CLB05-31.* Olivine in the lherzolite CLB05-31 shows large variations in Li concentrations (1.1 to 2.4 ppm) and δ^7Li values (−10.3 to 5.5; fig. 3; table 2). Figure 4*a* shows a profile across a 1000-μm-diameter Ol, with δ^7Li ranging from −10.3 to 5.5. Li concentrations also show zoning in this grain, with values of 1.1 ppm in the rim to ~2.3 ppm in the core. A similar pattern of isotopic and elemental zonation is also observed in other Ol grains. Orthopyroxene shows very weak zonation of δ^7Li (approximately −8.8 to approximately −5.4) but clear zonation of Li (0.7~6.3 ppm). Clinopyroxene is enriched in Li (2.0~4.1 ppm) and variable in δ^7Li, ranging from −26.3 to −9.8, displaying a different style of zonation from Ol, where low Li concentrations in the cores are associated with much light δ^7Li (fig. 3).

Sample CLB05-50. Different from the lherzolite CLB05-31, Ol in the lherzolite CLB05-50 has a restricted range of Li concentrations (2.0~3.0 ppm) and δ^7Li (1.6~6.4; fig. 3; table 2). Clinopyroxene has slightly high Li concentrations (2.3~3.5 ppm) and a wide range of δ^7Li (0.3~5.5; fig. 3; table 2). Orthopyroxene displays large variations in Li con-

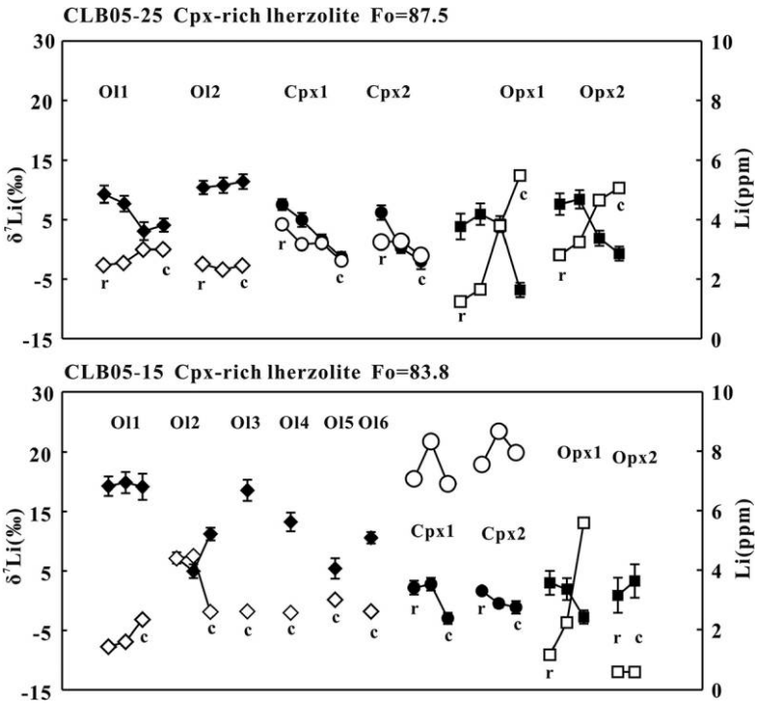

Figure 5. Profiles of Li concentrations and isotopic compositions of olivine (Ol), orthopyroxene (Opx), and clinopyroxene (Cpx) in the Beiyan Cpx-rich lherzolites analyzed by secondary ion mass spectroscopy. Open and filled symbols represent Li concentrations and δ^7Li, respectively. c = core; r = rim.

centrations (0.6~5.7 ppm) and δ^7Li (−12.2~12.3). An isotope transect across this big Opx grain (3.5 mm) shows a more complex zonation (fig. 4*b*). The rims yield δ^7Li of 9.7, and the core of the grain is anomalously light (δ^7Li of approximately −4.4). There are significant troughs of δ^7Li (−10.6 and −12.2) between the core and the respective edges of the crystals. Again, there is a clear negative correlation between Li concentration and δ^7Li value (fig. 4*b*).

Cpx-Rich Lherzolite. *Sample CLB05-25.* Olivine shows a homogeneous Li abundance (2.3~3.0 ppm). The δ^7Li values (5.0~13.3) of Ol are higher than those of upper mantle (2~6; Tomascak 2004; Tomascak et al. 2008), on the basis of the isotopic compositions of oceanic basalts. Relative to Ol, Cpx and Opx show a bit greater range (2.6~3.8 and 1.2~5.5 ppm, respectively) and display slightly larger intragrain variation (fig. 5; table 2). Orthopyroxene has a pattern of elemental and isotopic zonation similar to that of lherzolite CLB05-31 (fig. 5). The Cpx grains show different styles of zonation from Opx (fig. 5). The Li concentrations and δ^7Li values in Cpx are consistently increasing from core to rim.

Sample CLB05-15. The Li concentrations (1.4~4.5 ppm) and isotopic compositions (7.4~22.0) in Ol from sample CLB05-15 are highly variable from grain to grain (fig. 5; table 2). Olivine with fracture (Ol2, Ol4, Ol5, Ol6; fig. 6) displays low δ^7Li (7.4~15.7), whereas Ol without fracture (Ol1, Ol3; fig. 6) has markedly high δ^7Li (20.6~22.0). Indeed, the Li isotopic compositions of Ol greatly exceed those reported for fertile spinel and garnet peridotites elsewhere (Seiz and Woodland 2000; Seiz et al. 2004; Jeffcoate et al. 2007; Rudnick et al. 2007; Tang et al. 2007; Zhang et al. 2010; Gao et al. 2011). Clinopyroxene has high Li concentrations, of 6.9~8.7 ppm, while Opx exhibits even larger Li variation, ranging from 0.6 to 5.6 ppm (fig. 5; table 2).

Wehrlite. Olivine in two wehrlites (CLB05-80 and CLB05-35) is enriched in Li (2.4~4.2 ppm) and variable in δ^7Li, ranging from approximately −5.9 to approximately 8.6. Clinopyroxene also shows large variations in Li concentrations (0.7~7.2 ppm). The sieve-textured Cpx in wehrlite CLB05-80 shows significantly lower Li concentrations (0.7~1.8 ppm) than the well-defined one (3.6~6.0 ppm; fig. 7; table 2).

Discussion

Large and apparent variations in Li abundances and isotopic compositions have been observed on in-

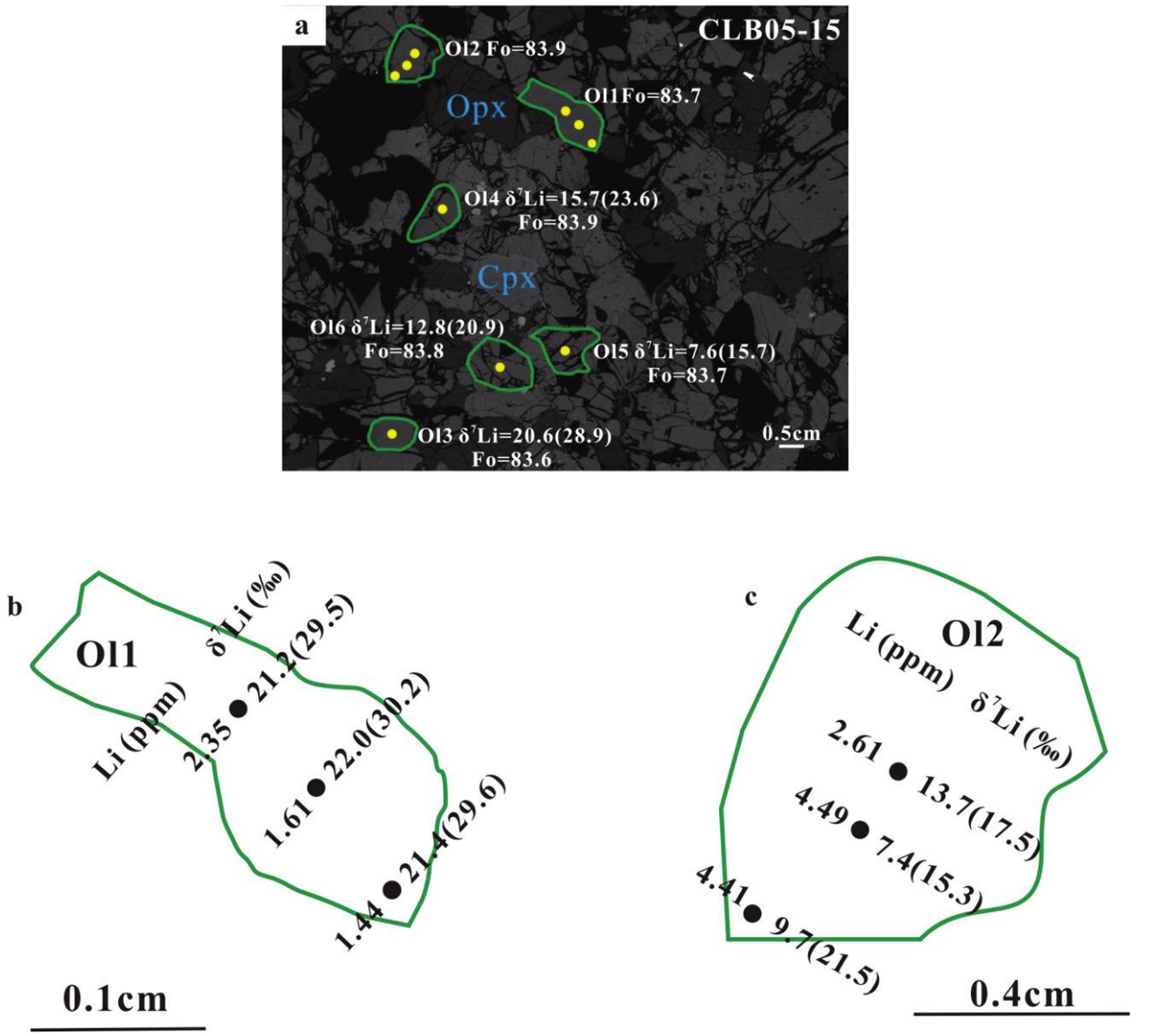

Figure 6. *a*, Backscattered electron micrograph of clinopyroxene (Cpx)–rich lherzolite CLB05-15 showing the position of the Li isotopic and Li concentration measurements determined by secondary ion mass spectroscopy (SIMS). *b*, *c*, Trace outlines of olivine (Ol) crystal fragments showing the position of the Li isotopic and Li concentration measurements determined by SIMS. Opx = orthopyroxene.

tragrain and intersample scales in the Beiyan xenoliths (figs. 3, 5, 7). In the following discussion, we focus first on intragrain Li isotope fractionation and the potential factors controlling the fractionation and then on intersample Li isotope fractionation. Finally, we discuss the potential implications for intersample heterogeneity together with other geochemical data.

Intragrain Fractionation. Lithium is a moderately incompatible element (Brenan et al. 1998*a*, 1998*b*) and has relatively high diffusivity, with ^{6}Li diffusing faster than ^{7}Li in mantle minerals (Coogan et al. 2005; Dohmen et al. 2010; Richter et al. 2014). Seitz and Woodland (2000) reported that the compositional ranges of Li in Ol and pyroxenes in fertile to moderately depleted mantle are 1.0~1.8 and 0.5~1.3 ppm, respectively, and estimated a bulk Li content of 1.0~1.5 ppm for the upper mantle. An average δ^{7}Li of 3.5 was proposed as a value for the upper mantle on the basis of fertile peridotites (Jeffcoate et al. 2007; Pogge von Strandmann et al. 2011), which is consistent with that of MORBs

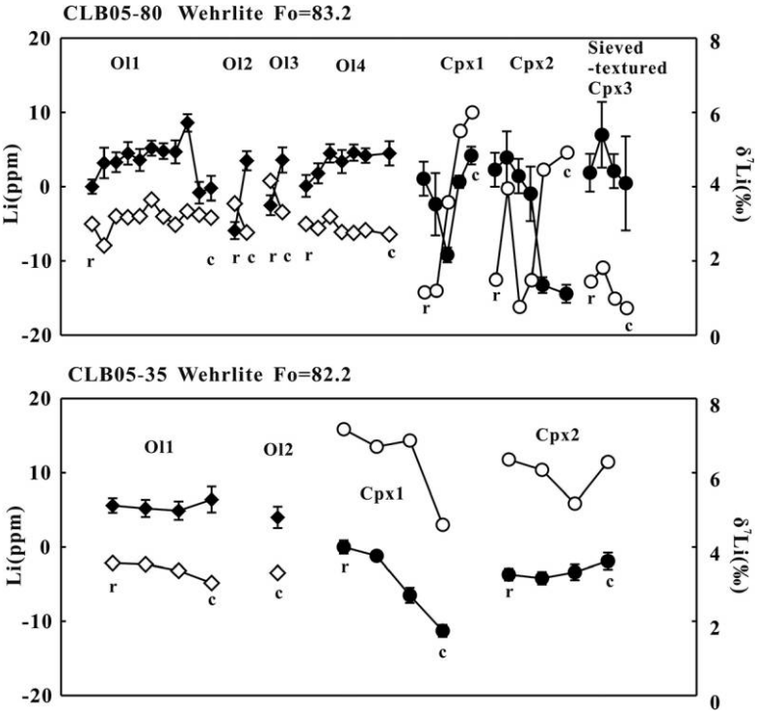

Figure 7. Profiles of Li concentrations and isotopic compositions of olivine (Ol) and clinopyroxene (Cpx) in the Beiyan wehrlites analyzed by secondary ion mass spectroscopy. Open and solid symbols represent Li concentrations and δ^7Li, respectively. c = core; r = rim.

(Tomascak 2004; Tomascak et al. 2008). Indeed, Li isotopes can be strongly fractionated due to diffusive kinetic fractionation in peridotites, which could occur during interaction of the xenoliths with host magmas and infiltrating melts (Nishio et al. 2004; Jeffcoate et al. 2007; Rudnick and Ionov 2007; Tang et al. 2007, 2011, 2012, 2014; Aulbach et al. 2008; Aulbach and Rudnick 2009; Zhang et al. 2010; Su et al. 2012, 2014) or during slow cooling (Ionov and Seitz 2008; Gao et al. 2011).

Basically, most olivines have relatively low Li contents and normal mantle-like δ^7Li, similar to MORBs (Tomascak et al. 2008), whereas Cpx and Opx have high Li abundances but low δ^7Li. The low δ^7Li in the pyroxenes could result from diffusion-driven kinetic isotope fractionation due to Li ingress from melt or host magma (e.g., Jeffcoate et al. 2007; Rudnick and Ionov 2007) and/or from coexisting Ol by subsolidus intermineral Li-redistribution during slow cooling (e.g., Ionov and Seitz 2008; Gao et al. 2011). In this study, most Cpx grains from Beiyan peridotites show isotopically light cores with Li concentrations lower than those in the heavy rims, similar to the fertile Vitim xenoliths (figs. 3, 5, 7; Jeffcoate et al. 2007). This suggests that ^{6}Li preferentially diffuses into Cpx from the entraining magma or during related intrusive magmatism, shortly before or coincident with transport of the mantle wall-rock fragment to the surface (Jeffcoate et al. 2007; Ionov and Seitz 2008; Gao et al. 2011). The W-shape profile seen in the coarse-grained Opx from the xenolith CLB05-50 (fig. 4*b*) may also be explained as the result of diffusional processes during entrainment (Jeffcoate et al. 2007; Richter et al. 2014).

The complex patterns of Li isotope zonation in Ol (fig. 4*a*) from sample CLB05-31 show isotopically heavy rims with Li concentrations lower than those in the light cores (δ^7Li of approximately −10.3). The δ^7Li_{Ol} value of the core in this sample is much lower than normal mantle (Jeffcoate et al. 2007; Pogge von Strandmann et al. 2011). Thus, the redistribution of Li between minerals during slow cooling, which show low δ^7Li in Cpx but normal mantle-like (or high) δ^7Li in Ol, cannot sufficiently explain the isotopically light core of Ol in this study. If low δ^7Li in mantle olivines were produced by diffusion-driven fractionation of Li isotopes during the interaction of the xenoliths with host magmas, they should show isotopically light cores with

Li concentrations lower than those in the heavy rims, which are different from those in sample CLB05-31. Lundstrom et al. (2005) reported that differential diffusion of Li isotopes within the melt phase alone can readily explain isotopic compositions of δ^7Li of approximately −20 in melts invading peridotite. Thus, the most likely explanation for the isotopically light core is that the source of Li was a relatively small volume of grain-boundary fluid or melts with low δ^7Li value. Then, the isotopically heavy rim with low Li concentration may be best explained by the redistribution of Li between minerals during slow cooling. However, Ol grain lost Li in two boundary layers but retained a relatively undisturbed core (fig. 4*a*). Olivines in other Beiyan peridotites are generally homogeneous in Li concentration and have restricted variation in δ^7Li (figs. 3, 5, 7).

Because of a much faster diffusion rate (approximately four orders of magnitude) of Li in Cpx than in Ol (Gao et al. 2011), zoning patterns of Cpx may reflect very recent diffusion of Li into Cpx. We therefore focus the rest of our discussion on Li in Ol.

Intersample Li Isotopic Fractionation. Previous studies have shown that Ol generally has relatively low Li concentrations and normal mantle-like δ^7Li (Seitz and Woodland 2000; Jeffcoate et al. 2007), similar to MORBs (Tomascak 2004; Tomascak et al. 2008). Compared with published data for worldwide peridotites, Ol in the Beiyan xenoliths show limited variations in Li abundances and δ^7Li (fig. 8*a*). In this study, Ol in all samples has slightly higher Li concentrations (>2 ppm) and larger Li isotope variation (−10.3~22.0) than those in normal mantle. Previous studies have shown that Beiyan Cpx-rich lherzolites and wehrlites were formed by reactions of host lherzolites with melts, on the basis of detailed petrological and geochemical analyses (Xiao et al. 2010; Xiao and Zhang 2011). In fact, Li concentrations of Ol from Beiyan peridotites also show a systematic variation of wehrlites > Cpx-rich lherzolites > lherzolites. However, Ol in the Cpx-rich lherzolites has much heavier δ^7Li than that in the lherzolites and wehrlites (fig. 8; table 2). A number of processes can potentially disturb Li isotope ratios of Ol, such as melt extraction (Seitz and Woodland 2000), interaction of the xenoliths with host magmas and infiltrating melts (Nishio et al. 2004; Jeffcoate et al. 2007; Rudnick and Ionov 2007; Tang et al. 2007, 2011, 2012; Aulbach et al. 2008; Aulbach and Rudnick 2009; Zhang et al. 2010; Su et al. 2012), and slow cooling (Ionov and Seitz 2008; Gao et al. 2011). Because of the moderate incompatibility of Li, melt extraction would decrease

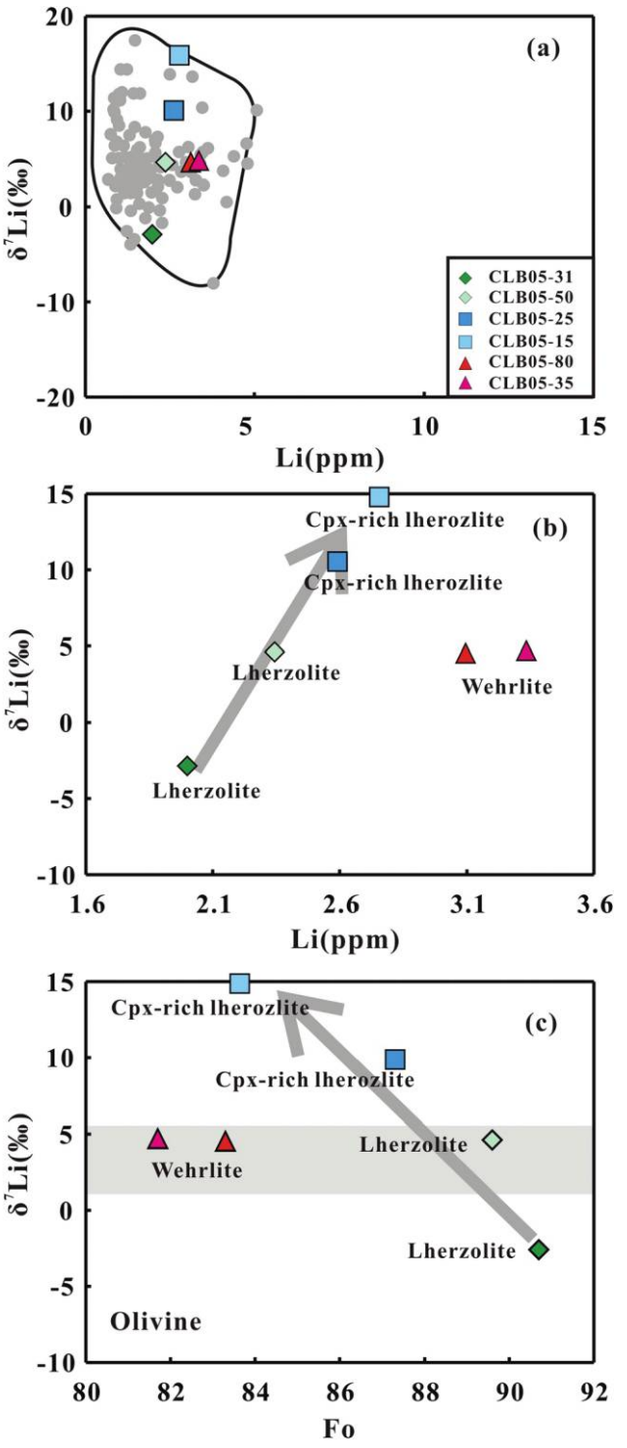

Figure 8. *a*, *b*, Variation in Li concentrations with olivine (Ol) δ^7Li in the Beiyan xenoliths compared with worldwide data. *c*, Variation in δ^7Li as a function of Fo concentration. The solid field represents data for worldwide Ol (Nishio et al. 2004; Seitz et al. 2004; Magna et al. 2006; Jeffcoate et al. 2007; Rudnick and Ionov 2007; Tang et al. 2007, 2011, 2012; Wagner and Deloule 2007; Ionov and Seitz 2008; Aulbach and Rudnick 2009; Halama et al. 2009; Zhang et al. 2010). Cpx = clinopyroxene.

concentrations in all minerals (Seitz and Woodland 2000). However, Ol in Beiyan peridotites has relatively high Li concentrations (>2 ppm), and the effect of different degrees of melt extraction on Li isotopic variation in the Beiyan peridotites can be ruled out. Additionally, Li will diffuse from Ol into Cpx with decreasing temperature at mantle depth, resulting in distinctly high-δ^7Li Ol and low-δ^7Li Cpx in mantle peridotites but low Li contents in Ol (Ionov and Seitz 2008; Gao et al. 2011). However, most olivines in the Beiyan peridotites are high in δ^7Li and have Li abundances higher than those of normal mantle (figs. 3, 5, 7), implying a small effect of diffusive fractionation on the compositions of olivines during their entrainment into the host magmas and transportation to the surface. The other two processes will be explored below.

Cpx-Rich Lherzolites with High δ^7Li of Ol. Olivine in the Cpx-rich lherzolite samples CLB05-25 and CLB05-15 displays much heavier δ^7Li than that in lherzolites and peridotites reported elsewhere (Seiz and Woodland 2000; Seiz et al. 2004; Jeffcoate et al. 2007; Rudnick et al. 2007; Tang et al. 2007; Zhang et al. 2010; Gao et al. 2011). Petrological and geochemical studies suggest that the Beiyan Cpx-rich lherzolites were produced by interaction of lherzolites with silicate melt, which caused partial replacements of Opx by Cpx and moderate Fe enrichments (Xiao et al. 2010). In particular, δ^7Li values correlate positively with Li concentrations (fig. 8*b*) and negatively with Fo (fig. 8*c*) from lherzolites to Cpx-rich lherzolites, indicating that these Cpx-rich lherzolites are the products of reaction between an isotopically heavy Li- and Fe-rich melt and lherzolites. Interestingly, different Ol grains with the same Fo contents and same sizes in the Cpx-rich lherzolite sample CLB05-15 show different δ^7Li values and Li concentrations. These scenarios may indicate that high δ^7Li values in the Cpx-rich lherzolites resulted from precipitation of residual, isotopically heavy melts that had lost ^{6}Li during earlier diffusion due to a slower Li diffusion rate in Ol than in Cpx (Rudnick and Ionov 2007; Wagner and Deloule 2007; Aulbach et al. 2009).

Yang et al. (2009) and Zhao et al. (2012) reported Mg and Fe isotopic compositions of the Beiyan peridotites. A negative correlation between $\delta^{57}Fe_{Ol}$ and $\delta^{26}Mg_{Ol}$ was observed in lherzolites and Cpx-rich lherzolites and was attributed to result from diffusion-driven Mg/Fe isotope fractionation in mantle minerals during melt-peridotite interaction (fig. 9*a*; Zhao et al. 2012). Additionally, Xiao et al. (2013) also reported new Mg isotopic compositions of Ol, Opx, and Cpx from the Beiyan peridotites. The occurrence of large intermineral Mg isotope

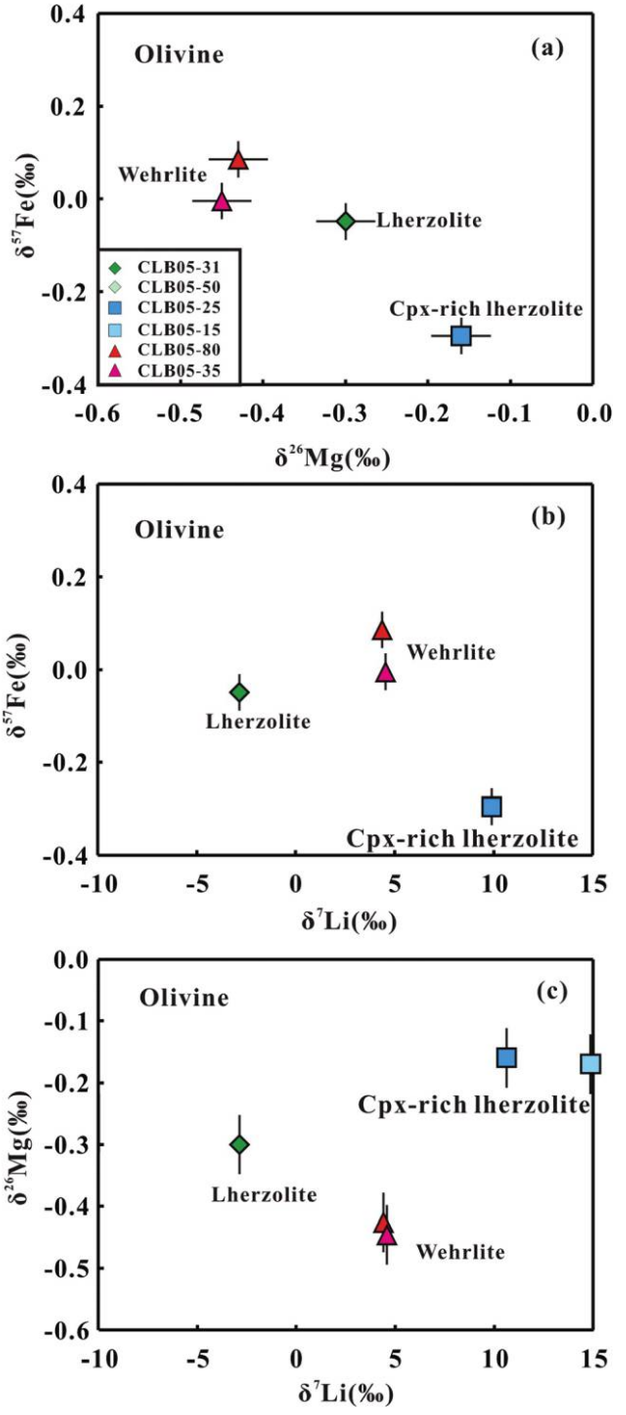

Figure 9. *a–c*, Mg, Fe, and Li isotope fractionations of olivine (Ol) in Beiyan peridotites. Shown are $^{87}Sr/^{86}Sr$ variations in clinopyroxene (Cpx) and Ol δ^7Li value for Beiyan peridotites. $\delta^{57}Fe_{Ol}$ and $\delta^{26}Mg_{Ol}$ data are from Yang et al. (2009), Zhao et al. (2012), and Xiao et al. (2010, 2013).

fractionation between coexisting pyroxenes and Ol in most Cpx-rich lherzolites has been ascribed to kinetic isotope fractionation during melt-peridotite interaction. There appears to be a positive covariation between δ^7Li_{Ol} and $\delta^{26}Mg_{Ol}$ and a negative covariation between δ^7Li_{Ol} and $\delta^{57}Fe_{Ol}$ from lherzolite to Cpx-rich lherzolite (fig. 9*b*, 9*c*). In particular, Ol δ^7Li values increase with increasing Li concentration and decreasing Fo contents (fig. 8*b*, 8*c*). All these features suggest that Li is also affected by diffusive processes, and the heavy Ol δ^7Li values may reflect diffusion-driven kinetic isotope fractionation during melt-rock interaction.

Wehrlite with High Li Concentrations of Ol. Relative to Cpx-rich lherzolites, the olivines of two wehrlites show similar Li concentrations and δ^7Li values (fig. 7; table 2). Previous studies have shown that the Beiyan wehrlites experienced multistage melt-peridotite interactions, as evidenced by extremely low Fo (<84) and the occurrence of apatite and calcite. Their Li concentrations are apparently higher than those of normal mantle, while δ^7Li values are within the range of normal mantle, reflecting metasomatism of the peridotites by asthenospheric melt.

Conclusions

From the above-described investigations, we can draw the following conclusions.

First, SIMS isotopic profiles of Ol and pyroxenes in mantle xenoliths reveal Li isotopic zonation. The most common Li isotope profiles in Cpx, with rims having lighter δ^7Li and higher Li concentrations than the cores, may be best explained by more rapid diffusion of ^{6}Li into the mineral grains. More complex zoning patterns observed in some grains may result from multiple stages of isotopic fractionation.

Second, the Li isotopic compositions of Ol in the variably metasomatized peridotites are highly variable. The olivines in the Cpx-rich lherzolites have lower Fo contents and show clearly higher δ^7Li than those of lherzolites and normal mantle value, reflecting diffusion-driven kinetic fractionation during melt-peridotite interaction. The olivines in the wehrlites with extremely low Fo contents show higher Li concentrations than those of normal mantle but have δ^7Li values similar to those of normal mantle, thus reflecting metasomatism of the peridotites by asthenospheric melt.

ACKNOWLEDGMENTS

We thank G.-Q. Tang and Y. Liu for their assistance in the measurement of the Li isotope, Q. Mao and Y.-G. Ma for their assistance in electron probe microanalyzer analyses, and W. Yang, P.-F. Zhang, and B. Zhu for discussions. Constructive and detailed comments from F. Richter and Editor D. B. Rowley are greatly appreciated. This research was financially supported by the National Natural Science Foundation of China (grant 91214203 to J.-F. Ying, grant 41273020 to Y. Xiao, and grant 91014007 to H.-F. Zhang).

REFERENCES CITED

Aulbach, S., and Rudnick, R. L. 2009. Origins of non-equilibrium lithium isotope fractionation in xenolithic peridotite minerals: examples from Tanzania. Chem. Geol. 258:17–27.

Aulbach, S.; Rudnick, R. L.; and McDonough, W. F. 2008. Li-Sr-Nd isotope signatures of the plume and cratonic lithospheric mantle beneath the margin of the rifted Tanzanian craton (Labait). Contrib. Mineral. Petrol. 155:79–92.

Beck, P.; Chaussidon, M.; Barrat, J. A.; Gillet, P.; and Bohn, M. 2006. Diffusion induced Li isotopic fractionation during the cooling of magmatic rocks: the case of pyroxene phenocrysts from nakhlite meteorites. Geochim. Cosmochim. Acta 70:4813–4825.

Bell, D. R.; Hervig, R. L.; Buseck, P. R.; and Aulbach, S. 2009. Lithium isotope analysis of olivine by SIMS: calibration of a matrix effect and application to magmatic phenocrysts. Chem. Geol. 258:5–16.

Brenan, J. M.; Neroda, E.; Lundstrom, C. C.; Shaw, H. F.; Ryerson, F. J.; and Phinney, D. L. 1998*a*. Behaviour of boron, beryllium, and lithium during melting and crystallization: constraints from mineral-melt partitioning experiments. Geochim. Cosmochim. Acta 62: 2129–2141.

Brenan, J. M.; Ryerson, F. J.; and Shaw, H. F. 1998*b*. The role of aqueous fluids in the slab-to-mantle transfer of boron, beryllium, and lithium during subduction: experiments and models. Geochim. Cosmochim. Acta 62:3337–3347.

Chu, Z. Y.; Wu, F. Y.; Walker, R. J.; Rudnick, R. L.; Pitcher, L.; Puchtel, I. S.; Yang, Y. H.; and Wilde, S. A. 2009. Temporal evolution of the lithospheric mantle beneath the eastern North China Craton. J. Petrol. 50:1857–1898.

Coogan, L. A.; Kasemann, S. A.; and Chakraborty, S. 2005. Rates of hydrothermal cooling of new oceanic upper

crust derived from lithium-geospeedometry. Earth Planet. Sci. Lett. 240:415–424.
Decitre, S. E.; Deloule, E.; Reisberg, L.; James, R.; Agrinier, P.; and Mevel, C. 2002. Behavior of Li and its isotopes during serpentinization of oceanic peridotites. Geochem. Geophys. Geosys. 3. doi:10.1029/2001GC000178.
Dohmen, R.; Kasemann, S. A.; Coogan, L.; and Chakraborty, S. 2010. Diffusion of Li in olivine. I. Experimental observations and a multi species diffusion model. Geochim. Cosmochim. Acta 74:274–292.
Gao, Y.; Snow, J. E.; Casey, J. F.; and Yu, J. 2011. Cooling-induced fractionation of mantle Li isotopes from the ultraslow-spreading Gakkel Ridge. Earth Planet. Sci. Lett. 301:231–240.
Halama, R; Savov, I. P.; Rudnick, R. L.; and McDonough, W. F. 2009. Insights into Li and Li isotope cycling and sub-arc metasomatism from veined mantle xenoliths, Kamchatka. Contrib. Mineral. Petrol. 158:197–222.
Ionov, D. A., and Seitz, H. M. 2008. Lithium abundances and isotopic compositions in mantle xenoliths from subduction and intra-plate settings: mantle sources vs. eruption histories. Earth Planet. Sci. Lett. 266:316–331.
Jeffcoate, A. B.; Elliott, T.; Kasemann, S. A.; Ionov, D.; Cooper, K.; and Brooker, R. 2007. Li isotope fractionation in peridotites and mafic melts. Geochim. Cosmochim. Acta 71:202–218.
Lundstrom, C. C.; Chaussidon, M.; Hsui, A. T.; Kelemen, P.; and Zimmerman, M. 2005. Observations of Li isotopic variations in the Trinity ophiolite: evidence for isotopic fractionation by diffusion during mantle melting. Geochim. Cosmochim. Acta 69:735–751.
Magna, T.; Wiechert, U.; and Halliday, A. N. 2006. New constraints on the lithium isotope compositions of the Moon and terrestrial planets. Earth Planet. Sci. Lett. 243:336–353.
Marks, M. A. W.; Rudnick, R. L.; McCammon, C.; Vennemann, T.; and Markl, G. 2007. Arrested kinetic Li isotope fractionation at the margin of the Ilímaussaq complex, South Greenland: evidence for open system processes during final cooling of peralkaline igneous rocks. Chem. Geol. 246:207–230.
Marschall, H. R.; Pogge von Strandmann, P. A. E.; Seitz, H. M.; Elliott, T.; and Niu, Y. 2007. The lithium isotopic composition of orogenic eclogites and deep subducted slabs. Earth Planet. Sci. Lett. 262:563–580.
Nishio, Y.; Shun'ichi, N.; Yamamoto, J.; Sumino, H.; Matsumoto, T.; Prikhod'ko, V. S.; and Arai, S. 2004. Lithium isotopic systematics of the mantle-derived ultramafic xenoliths: implications for EM1 origin. Earth Planet. Sci. Lett. 217:245–261.
Parkinson, I. J.; Hammond, S. J.; James, R. H.; and Rogers, N. W. 2007. High temperature lithium isotope fractionation: insights from lithium isotope diffusion in magmatic systems. Earth Planet. Sci. Lett. 257:609–621.
Peng, Z. C.; Zartman, R. E.; Futa, K.; and Chen, D. G. 1986. Pb-isotopic, Sr-isotopic and Nd-isotopic systematics and chemical characteristics of Cenozoic basalts, eastern China. Chem. Geol. 59:3–33.
Pogge von Strandmann, P. A. E.; Elliott, T.; Marschall, H. R.; Coath, C.; Lai, Y. J.; Jeffcoate, A. B.; and Ionov, D. A. 2011. Variations of Li and Mg isotope ratios in bulk chondrites and mantle xenoliths. Geochim. Cosmochim. Acta 75:5247–5268.
Richter, F.; Watson, B.; Chaussidon, M.; Mendybaev, R.; and Ruscitto, D. 2014. Lithium isotope fractionation by diffusion in minerals. I. Pyroxenes. Geochim. Cosmochim. Acta 126:352–370.
Rudnick, R. L., and Ionov, D. A. 2007. Lithium elemental and isotopic disequilibrium in minerals from peridotite xenoliths from far-east Russia: product of recent melt/fluid-rock reaction. Earth Planet. Sci. Lett. 256:278–293.
Seitz, H. M.; Brey, G. P.; Lahaye, Y.; Durali, S.; and Weyer, S. 2004. Lithium isotopic signatures of peridotite xenoliths and isotopic fractionation at high temperature between olivine and pyroxenes. Chem. Geol. 212:163–177.
Seitz, H. M., and Woodland, A. B. 2000. The distribution of lithium in peridotitic and pyroxenitic mantle lithologies—an indicator of magmatic and metasomatic processes. Chem. Geol. 166:47–64.
Su, B. X.; Zhang, H. F.; Deloule, E.; Sakyi, P. A.; Xiao, Y.; Tang, Y. J.; Hu, Y.; Ying, J. F.; and Liu, P. P. 2012. Extremely high Li and low δ^7Li signatures in the lithospheric mantle. Chem. Geol. 292–293:149–157.
Su, B. X.; Zhang, H. F.; Deloule, E.; Vigier, N.; Hu, Y.; Tang, Y. J.; Xiao, Y.; and Sakyi, P. A. 2014. Distinguishing silicate and carbonatite mantle metasomatism by using lithium and its isotopes. Chem. Geol. 381:67–77.
Tang, Y. J.; Zhang, H. F.; Deloule, E.; Su, B. X.; Ying, J. F.; Santosh, M.; and Xiao, Y. 2014. Abnormal lithium isotope composition from the ancient lithospheric mantle beneath the North China Craton. Sci. Rep. 4:4274.
Tang, Y. J.; Zhang, H. F.; Deloule, E.; Su, B. X.; Ying, J. F.; Xiao, Y.; and Hu, Y. 2012. Slab-derived lithium isotopic signatures in mantle xenoliths from northeastern North China Craton. Lithos 149:79–90.
Tang, Y. J.; Zhang, H. F.; Nakamura, E.; Moriguti, T.; Kobayashi, K.; and Ying, J. F. 2007. Lithium isotopic systematics of peridotite xenoliths from Hannuoba, North China Craton: implications for melt-rock interaction in the considerably thinned lithospheric mantle. Geochim. Cosmochim. Acta 71:4327–4341.
Tang, Y. J.; Zhang, H. F.; Nakamura, E.; and Ying, J. F. 2011. Multistage melt/fluid-peridotite interactions in the refertilized lithospheric mantle beneath the North China Craton: constraints from the Li-Sr-Nd isotopic disequilibrium between minerals of peridotite xenoliths. Contrib. Mineral. Petrol. 161:845–861.
Teng, F. Z.; McDonough, W. F.; Rudnick, R. L.; and Walker, R. J. 2006. Diffusion-driven extreme lithium

isotopic fractionation in country rocks of the Tin Mountain pegmatite. Earth Planet. Sci. Lett. 243:701–710.

Tomascak, P. B. 2004. Developments in the understanding and application of lithium isotopes in the earth and planetary sciences. *In* Johnson, C. M.; Beard, B. I.; and Albarede, F., eds. Geochemistry of non-traditional stable isotope. Reviews in Mineralogy and Geochemistry. Mineral. Soc. Am. 55:153–195.

Tomascak, P. B.; Langmuir, C. H.; le Roux, P. J.; and Shirey, S. B. 2008. Lithium isotopes in global mid-ocean ridge basalts. Geochim. Cosmochim. Acta 72: 1626–1637.

Wagner, C., and Deloule, E. 2007. Behaviour of Li and its isotopes during metasomatism of French Massif Central lherzolites. Geochim. Cosmochim. Acta 71:4279–4296.

Xiao, Y.; Teng, F. Z.; Zhang, H. F.; and Yang, W. 2013. Large magnesium isotopic variations in peridotite xenoliths from eastern North China Craton: product of melt-rock interaction. Geochim. Cosmochim. Acta 115:241–261.

Xiao, Y., and Zhang, H. F. 2011. Effects of melt percolation on platinum group elements and Re-Os systematics of peridotites from the Tan-Lu fault zone, eastern North China Craton. J. Geol. Soc. Lond. 168:1201–1214.

Xiao, Y.; Zhang, H. F.; Fan, W. M.; Ying, J. F.; Zhang, J.; Zhao, X. M.; and Su, B. X. 2010. Evolution of lithospheric mantle beneath the Tan-Lu fault zone, eastern North China Craton: evidence from petrology and geochemistry of peridotite xenoliths. Lithos 117: 229–246.

Xu, J. W.; Zhu, G.; Tong, W. X.; Cui, K. R.; and Liu, Q. 1987. Formation and evolution of the Tancheng-Lujiang wrench fault system: a major shear system to the northwest of the Pacific Ocean. Tectonophysics 134:273–310.

Xu, Y. G.; Mercier, J. C. C.; Menzies, M. A.; Ross, J. V.; Harte, B.; Lin, C. Y.; and Shi, L. B. 1996. K-rich glass-bearing wehrlite xenoliths from Yitong, northeastern China: petrological and chemical evidence for mantle metasomatism. Contrib. Mineral. Petrol. 125:406–420.

Xu, Y. G.; Ross, J. V.; and Mercier, J. C. C. 1993. The upper-mantle beneath the continental rift of Tanlu, eastern China—evidence for the intra-lithospheric shear zones. Tectonophysics 225:337–360.

Yang, W.; Teng, F. Z.; and Zhang, H. F. 2009. Chondritic magnesium isotopic composition of the terrestrial mantle: a case study of peridotite xenoliths from the North China Craton. Earth Planet. Sci. Lett. 288:475–482.

Ying, J. F.; Zhang, H. F.; Kita, N.; Morishita, Y.; and Shimoda, G. 2006. Nature and evolution of Late Cretaceous lithospheric mantle beneath the eastern North China Craton: constraints from petrology and geochemistry of peridotitic xenoliths from Junan, Shandong Province, China. Earth Planet. Sci. Lett. 244:622–638.

You, C. F.; Chan, L. H.; Gieskes, J. M.; and Klinkhammer, G. P. 2003. Seawater intrusion through the oceanic crust and carbonate sediment in the equatorial Pacific: lithium abundance and isotopic evidence. Geophys. Res. Lett. 30:2120.

Zhang, H. F.; Deloule, E.; Tang, Y. J.; and Ying, J. F. 2010. Melt/rock interaction in remains of refertilized Archean lithospheric mantle in Jiaodong Peninsula, North China Craton: Li isotopic evidence. Contrib. Mineral. Petrol. 160:261–277.

Zhang, J.; Zhang, H. F.; Kita, N.; Shimoda, G.; Morishita, Y.; Ying, J. F.; and Tang, Y. J. 2011. Secular evolution of the lithospheric mantle beneath the eastern North China Craton: evidence from peridotitic xenoliths from Late Cretaceous mafic rocks in the Jiaodong region, east-central China. Int. Geol. Rev. 53:182–211.

Zhao, G. C.; Wilde, S. A.; Sun, M.; Li, S. Z.; Li, X. P.; and Zhang, J. 2008. SHRIMP U-Pb zircon ages of granitoid rocks in the Lüliang Complex: implications for the accretion and evolution of the Trans–North China Orogen. Precambrian Res. 160:213–226.

Zhao, X. M.; Zhang, H. F.; Zhu, X. K.; Tang, S. H.; and Yan, B. 2012. Iron isotope evidence for multistage melt-peridotite interactions in the lithospheric mantle of eastern China. Chem. Geol. 292–293:127–139.

Zheng, J. P.; Griffin, W. L.; O'Reilly, S. Y.; Yu, C. M.; Zhang, H. F.; Pearson, N.; and Zhang, M. 2007. Mechanism and timing of lithospheric modification and replacement beneath the eastern North China. Geochim. Cosmochim. Acta 71:5203–5225.

Zheng, J. P.; O'Reilly, S. Y.; Griffin, W. L.; Lu, F. X.; and Zhang, M. 1998. Nature and evolution of Cenozoic lithospheric mantle beneath Shandong peninsula, Sino-Korean Craton, eastern China. Int. Geol. Rev. 40:471–499.